Journal of Ceramic Processing Research. Vol. 22, No. 6, pp. 665~674 (2021)
(Received 27 May 2021, Received in revised form 10 September 2021, Accepted 11 September 2021)
https://doi.org/10.36410/jcpr.2021.22.6.665

J O U R N A L O F
Ceramic Processing Research

Combined effect of Fe_2O_3 and Cr_2O_3 on the structure and properties of glass-ceramics prepared from Baotou steel blast furnace slag

Guangyu Wang[a], Yongsheng Du[a,*], Jie Ma[a], Hongxia Zhang[a], Shunli Ouyang[b], Leibo Deng[b], Hua Chen[a] and Ming Zhao[b]

[a]*College of Science, Inner Mongolia University of Science and Technology, Baotou 014010, China*
[b]*Key Laboratory of Integrated Exploitation of Bayan Obo Multi-Metallic Resources, Inner Mongolia University of Science and Technology, Baotou 014010, China*

CaO-MgO-Al_2O_3-SiO_2 glass-ceramics were successfully prepared using Baotou Steel BFS as the raw materials, choosing Fe_2O_3 and Cr_2O_3 as nucleating agents. This paper focused on analyzing the combined effect of Fe_2O_3 and Cr_2O_3 on the structure and properties of the glass-ceramics. Experimental results showed that the crystallization mechanism of glass-ceramics converted surface crystallization into bulk crystallization and the main crystalline phase of glass-ceramics changed gradually from augite to diopside with the decrease of Fe_2O_3/Cr_2O_3 ratios. Therefore, an appropriate ratio of Fe_2O_3/Cr_2O_3 can act as nuclei for crystallization of augite with integrated interlocking crystal structure and the physicochemical properties of glass-ceramic can be improved. Consequently, the fracture mode of glass-ceramic was changed from intercrystalline to mixed transcrystalline/ intercrystalline and therefore the average crack length can be shortened. Glass-ceramic with Fe_2O_3/Cr_2O_3 ratio of 1 had a high bending strength of 138.93 MPa, Vickers hardness of 7.51 GPa and acid resistance of 97.75%.

Keywords: Baotou steel blast furnace slag, glass-ceramic, combined effect, composite nucleating agents.

Table of Abbreviations

BFS	Blast furnace slag
CMAS	CaO-MgO-Al_2O_3-SiO_2
BO	Bridging oxygen
NBO	Non-bridging oxygen
DSC	Differential scanning calorimetry
SEM	Scanning electron microscope
XRD	X-ray diffraction

Introduction

The rapid development of national economic construction has brought about the widespread attention in the field of the environment and ecology due to the discharge of a large amount of solid wastes in the process of production. The extremely high resource consumption lead to the huge amount of emissions and accumulation of all kinds of mining waste, tailings after beneficiation, blast furnace slag (BFS), steel slag, fly ash, etc. These solid wastes have occupied a large number of land resources, destroyed the ecological environment and produced serious secondary pollution. Therefore, the comprehensive utilizations of the above-mentioned solid wastes are an effective means to solve the problem of environmental pollution. Because the solid wastes can provide the main components for the preparation of glass-ceramics, the glass-ceramics made of solid wastes exhibit excellent mechanical and stable chemical properties, and it can be widely used as transportation pipeline in various fields, e. g. chemical industry, metallurgy, electric power. Thus, the preparation of glass-ceramics realizes the environmental protection, high return and efficient utilization of solid waste [1-3].

Among all kinds of solid wastes, BFS is a hazardous metallurgical waste generated in the ironmaking process. The output of China's BFS is about 180-220 million tons, accounting for about half of the waste in the steel industry [4]. The large amounts of BFS accumulated not only occupy a large area of land but also seriously pollute the natural environment. Because the principal constituents of BFS are SiO_2, CaO, Al_2O_3 and MgO with a small amount of symbiotic (associated) metal elements such as Cr, Mn, Ti, K, and Na, as in Baotou Steel BFS, it is very suitable to prepare CaO-MgO-Al_2O_3-SiO_2 (CMAS) glass-ceramics. Several results of preparing glass-ceramics from BFS as the basic material have been widely reported and these glass-ceramics exhibited excellent mechanical properties as well as chemical properties. Zhao et al. studied the glass-ceramics prepared from molten BFS using CaF_2 as the nucleating agent and found that the bending strength of glass-ceramics samples increased up to 120 MPa [5]. Deng et al. reported that high-performance glass-ceramics with acid resistance of 97.91% and bending

*Corresponding author:
Tel :+86-472-5954358
Fax: +86-472-5954358
E-mail: dys1111@imust.edu.cn

strength of 210.27 MPa can be prepared from BFS, Bayan Obo tailings, and fly ash using Fe_2O_3 as the nucleating agent [6]. Generally speaking, addition of nucleating agents is necessary for the preparation of glass-ceramics from BFS due to the lack of effective nucleating agents in BFS. For example, the nucleating agents Cr_2O_3, Fe_2O_3, and TiO_2 have a very important influence on the crystallizability and properties of low-titanium BFS glass-ceramics. Khater et al. found that Cr_2O_3 and TiO_2 exhibited a remarkable ability to promote the homogeneous nucleation of glass-ceramics based on BFS [7]. Rezvani et al. found that Cr_2O_3, Fe_2O_3, and TiO_2 can effectively enhance the bulk crystallization of glass-ceramics [8]. Other relevant research results also have shown that Cr_2O_3 and Fe_2O_3 were two effective nucleating agents in the glass-ceramic system. Shi et al. investigated the nucleation and crystallization mechanism in a Cr_2O_3-doped CMAS glass-ceramic, and it was found that Cr_2O_3 can induce the formation of diopside in CAMS glass-ceramics through precipitation of $MgCr_2O_4$ spinel crystals [9]. Mohaghegh et al. researched the influence of Fe_2O_3 on the crystallization characteristics of lithium titanium phosphate glass-ceramics. Their results showed that Fe_2O_3 can be used as a network modifier in the glass structure and can weaken the strength of the glass phase [10]. In particular, He et al. reported that the proper proportion of Cr_2O_3/Fe_2O_3 was helpful for cordierite to form hexagonal close-packed structure with fine grains and uniform distribution in MgO-Al_2O_3-SiO_2-B_2O_3 glass-ceramic [11]. Therefore, the glass-ceramic showed excellent mechanical properties and this can be attributed to the combined effects of multiple nucleating agents Cr_2O_3 and Fe_2O_3 in the glass-ceramic. Marghussian et al. suggested that the multiple nucleating agents Cr_2O_3, Fe_2O_3, and TiO_2 can effectively enhance the nucleation of SiO_2-Al_2O_3-MgO-CaO(R_2O) glass systems [12]. However, the mechanism of influence of composite nucleating agents on the structure and properties of glass-ceramics still needs to be further studied. In this study, glass-ceramics were prepared from Baotou Steel BFS using the melting method. The effects of two different nucleating agents, Fe_2O_3 and Cr_2O_3, on the crystallization behavior and physicochemical properties were systematically studied. The purpose of this study was to investigate the combined effects of Fe_2O_3 and Cr_2O_3 on the structure and properties of glass-ceramics to determine the optimum mixture ratio of Fe_2O_3/Cr_2O_3. Furthermore, the objective of this study was to examine the solidification of Cr and Mn in glass-ceramics.

Material and Methods

CaO-MgO-Al_2O_3-SiO_2 (CMAS) glass-ceramics were prepared from a mixture which was composed of Baotou steel BFS, SiO_2, Na_2CO_3, MgO, Fe_2O_3 and Cr_2O_3 (chemical grade) by melting method, and the chemical composition of BFS was shown in Table 1. The composition of the base glass was chosen as 49.93%SiO_2, 23.01%CaO, 9.53%MgO and 7.29%Al_2O_3 (weight ratio) according to the phase diagram of augite and diopside and the detailed experimental design was shown in Table 2. For investigating the effect of Fe_2O_3/Cr_2O_3 ratios on nucleation, crystallization and properties of glass-ceramics, five batches (sample nos. FC1, FC2, FC3, FC4 and FC5) with different Fe_2O_3/Cr_2O_3 additions were prepared.

Process for preparing glass-ceramic mainly included four steps, glass melting, annealing, nucleation and crystallization. Firstly, the evenly mixed raw materials were placed in alumina crucibles melted at 1450°C for 3h. Subsequently, a small amount of melts were poured into an ice-water mixture directly for differential scanning calorimetry (DSC) examination, and the remaining melts were cast into preheated molds at 600 °C, placed in a separate electric furnace, and annealed at 600 °C for 5 h to eliminate any residual internal stress. Then, the specimens were cooled to room temperature in the furnace. Finally, glass-ceramics can be obtained by a two-step heat treatment method according to the result of DSC.

DSC (NETZSCH 449) was used to examine the thermo behaviors of the parent glasses in the range from room temperature to 1200 °C after heating at rates of 10 °C/min. According to the glass transition temperature (T_g) and crystallization exothermic peak temperature (T_p), that found by DSC, the nucleation and crystallization temperature of glass-ceramics can be determined. The crystalline phases of the glass-ceramic were determined by powder X-ray diffraction (XRD, PANalytical), applying Cu Kα radiation at room temperature. The surface morphology of glass-ceramics was observed with a field emission scanning electron microscope (FESEM, Supra 55, ZEISS). For FESEM analysis, the

Table 2. Ingredients of glass-ceramic

Sample	BFS	SiO_2	Na_2CO_3	MgO	Fe_2O_3	Cr_2O_3
FC1	64.02	27.77	2.43	3.15	2.63	0
FC2	64.02	27.77	2.43	3.15	1.97	0.66
FC3	64.02	27.77	2.43	3.15	1.315	1.315
FC4	64.02	27.77	2.43	3.15	0.66	1.97
FC5	64.02	27.77	2.43	3.15	0	2.63

Table 1. Chemical composition of BFS (wt%).

Composition	SiO_2	CaO	MgO	Al_2O_3	K_2O	Na_2O	TFe	TiO_2	MnO	REO
wt%	34.60	36.79	9.57	12.16	0.48	0.74	0.5	0.34	0.75	4.07

Note: REO denotes the sum of rare earth oxides in the BFS, including La_2O_3 (1.50 wt%) and CeO_2 (2.57 wt%).

samples were polished and etched with 5 wt% hydrofluoric acid (HF) solution for 75 s. The compositions of samples were identified by an energy dispersive spectrometer (EDS). The Si-O polymeric network structure of the glass samples were measured by Raman spectroscopy (InVia). The Vickers micro-hardness of glass-ceramics was investigated by Vickers hardness tester (HV-50A). The bulk densities of glass-ceramics were measured by the Archimedes method. Test for bending strength were provided by three-point bending method on a CSS-88000 electronic universal testing machine. The corrosion resistance tests were evaluated by measuring the mass of the glass-ceramics pellets with a particle size of 0.5-1.0 mm before and after the acid-base corrosion in 20 wt% H_2SO_4 solutions within water bath heating of 100 ºC. The corresponding calculation formulae was written as $K = m_2/m_1 \times 100\%$, where m_1 and m_2 were the mass before and after corrosion.

Results and Discussion

Thermal behavior analysis

The DSC curves of parent glasses with different Fe_2O_3/Cr_2O_3 ratios are given in Fig. 1. The glass transition temperature, T_g, ranged from 690 to 716 ºC, which can be determined according to the stepped endothermic curve, and the obvious exothermic peak corresponding to T_p ranged from 945 to 980 ºC. Both the T_g and T_p of glass-ceramics decrease with the decrease of Fe_2O_3/Cr_2O_3 ratios, which may result in a decrease in glass viscosity and an increase in crystallization characteristics [13-15]. This phenomenon is related to the different ratios of Fe_2O_3/Cr_2O_3 in glass-ceramics. As common nucleating agents, Fe_2O_3 and Cr_2O_3 can improve the nucleation and crystallization of glass-ceramics by forming magnetite or spinel. However, the influence of Fe_2O_3 and Cr_2O_3 on the glass network structure is different in the process of nucleation and crystallization of glass-ceramics. In general, iron ions have two valence states in glass-ceramics and the majority of iron ions exist in the Fe^{3+} state because the heat treatment of glass-ceramics is carried out in an oxidizing atmosphere. The presence of Fe^{2+} and Fe^{3+} is helpful for the formation of magnetite, which can form heterogeneous surfaces for subsequent crystallization of glass-ceramics [16]. The remaining Fe^{3+} can exist in the glass phase in the form of [FeO_4] tetrahedrons [17], which can increase the integrity of the glass network structure and thus increase the glass viscosity. As a result, the crystallization temperature moves toward higher temperature and the crystallization ability of the glass-ceramic is gradually weakened. Thus, surface crystallization of glass-ceramics may occur by adding the nucleating agent Fe_2O_3 [18]. However, Cr^{3+} does not participate in the formation of the glass network structure, and it may cause the chemical bonds of Si–O–Si or Si–O–Al in the silica network to break down

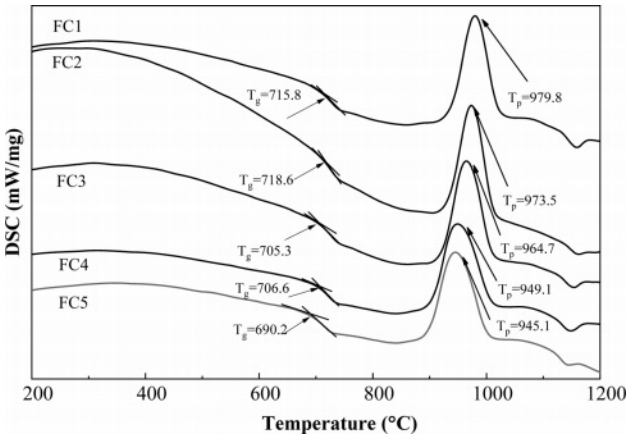

Fig. 1. DSC curves of the base glasses

owing to the high electric field characteristics of Cr^{3+} [19]. Meanwhile, Cr^{3+} has a strong chemical affinity with Mg^{2+} and Al^{3+}, thereby leading to the formation of a Cr-containing spinel, which can provide an interface for heterogeneous crystallization [20]. Therefore, in this experiment, with the decrease of Fe_2O_3/Cr_2O_3 ratios, both T_g and T_p show a significant decreasing trend. In addition, the nucleation and crystallization temperatures of the glass-ceramic can also be determined using DSC results. The annealed glass sample is heat-treated for 5 h at 750 ºC and 980 ºC for the nucleating and crystallization stages, respectively.

Phase formation

The crystal structures of glass-ceramics were determined from the powder XRD data and the results are shown in Fig. 2. Obvious diffraction peaks of the main crystalline phase can be observed in all samples, which indicates that both Fe_2O_3 and Cr_2O_3 can be used as effective nucleating agents to promote precipitation of the crystalline phase. It can be seen from Fig. 2(a) that the main crystalline phase of glass-ceramics changes gradually from diopside ($Ca(Mg,Al)(Si,Al)_2O_6$) in sample FC5 to augite ($Ca(Mg,Fe,Al)(Si,Al)_2O_6$) in sample FC1 with the increase of Fe_2O_3/Cr_2O_3 ratios. This phenomenon indicates that Fe^{3+} can enter the crystal lattice of diopside substitutionally replacing the Al^{3+} because of the similar ionic radii, which can lead to an increased lattice parameter of diopside due to a larger radius of Fe^{3+}. As a result, the interplanar spacing of the diopside increased and the diffraction peaks shifted to lower angles, as shown in Fig. 2(b). Meanwhile, it can be seen that the degree of crystallization of glass-ceramics is increased gradually with the decrease of Fe_2O_3/Cr_2O_3 ratios, which coincides with the decrease of T_g and T_p in the DSC results. This is because a small amount of Fe^{3+} can participate in the formation of the glass network with [FeO_4] tetrahedrons, which leads to an increase in glass viscosity and a slight decrease in crystallization. Furthermore, it should also be noted that the second

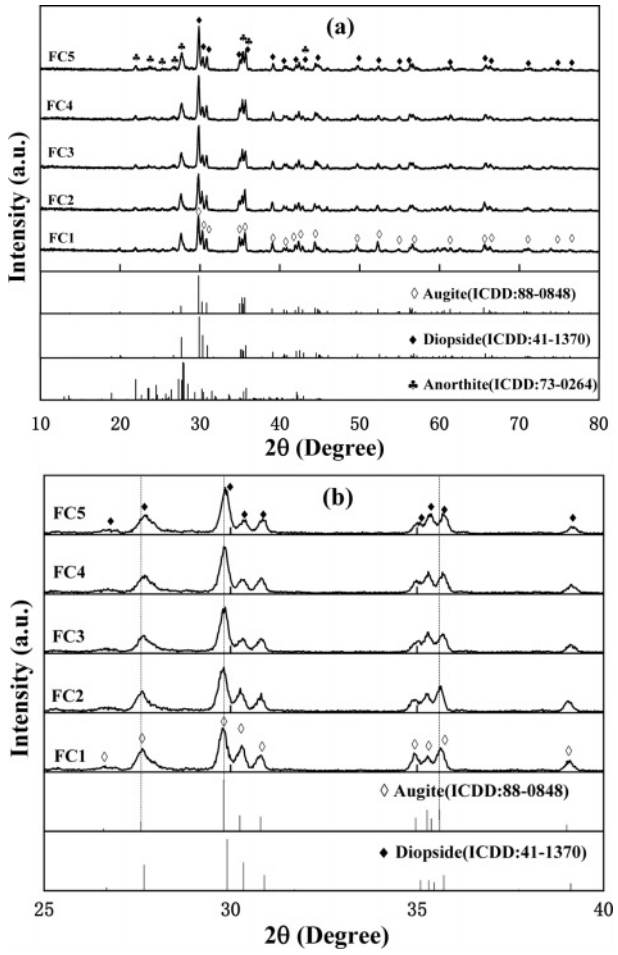

Fig. 2. XRD spectra of samples with different Fe_2O_3/Cr_2O_3 ratios: (a) normal views, (b) local enlarged views.

phase of anorthite ($Ca(Al_2Si_2O_8)$) can also appear in glass-ceramics, which may be attributed to the higher content of calcium in BFS.

Morphological characterization and element distribution

Fig. 3 shows the SEM images of glass-ceramics with different Fe_2O_3/Cr_2O_3 ratios. The dendrite crystal morphology with a high aspect ratio can be found in sample FC1 (using only Fe_2O_3 as a nucleating agent). With the decrease of Fe_2O_3/Cr_2O_3 ratios, the mean length of dendrite decreases gradually, and the shape of dendrite gradually changes into leaf-like morphology and finally becomes a short rod-like shape. The change of surface morphology of glass-ceramics is closely related to the different ratios of Fe_2O_3/Cr_2O_3. As a nucleating agent, the ability of Fe_2O_3 to promote nucleation and crystallization of glass-ceramics is weaker than that of Cr_2O_3. Cr_2O_3 can strongly promote the bulk crystallization of glass-ceramics by forming spinel nuclei, and the main crystalline phase of diopside/augite grows preferentially along the normal direction of the spinel surface in the form of dendrites. This growth mode contributes to the formation of an interlocking rod-shaped crystalline phase. The presence of Fe^{2+} and Fe^{3+} contributes to the formation of magnetite, thus promoting the nucleation and crystallization of glass-ceramics. Because Fe_2O_3 does not effectively induce bulk crystallization of glass-ceramics, the crystalline phase mainly grows from the surface to the inside along the temperature gradient direction. Thus, the dendrite crystal morphology with a high aspect ratio can be formed. Subsequently, with the decrease of Fe_2O_3/Cr_2O_3 ratios, the mode of crystallization of glass-ceramics changes from surface crystallization to bulk crystallization and the crystal morphology is transformed from developed dendrite to rod-like dendrite. However, excessive addition of Cr_2O_3 can increase the amount of precipitation of spinel, which will consume a certain amount of Mg^{2+}. As a result, the precipitation of the diopside/augite phase is restrained because of the decrease of Mg^{2+} in base glasses.

It is known from XRD spectra and SEM images that glass-ceramics are mainly composed of diopside/augite, anorthite, spinel, and glass phases. To determine further the distribution of elements in the crystal and glass phases, the BSE elemental mapping images of

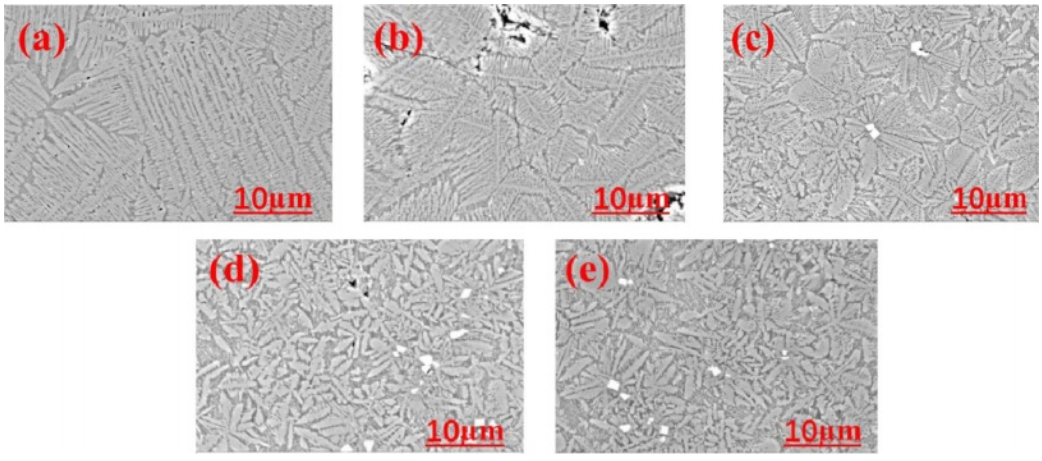

Fig. 3. SEM micrographs of glass-ceramics with different ratios of Fe_2O_3/Cr_2O_3: (a) FC1; (b) FC2; (c) FC3; (d) FC4; (e) FC5.

samples FC1, FC3, and FC5 were measured and the results are shown in Fig. 4. The glass phase is mainly enriched in Si, Al, and Na because $[SiO_4]$ tetrahedron or $[AlO_4]^-$ tetrahedron (Na^+ co-existed to balance the negative charge of $[AlO_4]^-$ tetrahedron) can be regarded as the basic unit of the glass network [21]. Because there is no Mg in the glass phase and anorthite, it can be found that the Mg-rich regions correspond to the main crystal phase of diopside/augite. Meanwhile, the concentrations of Cr and Mn can be discovered near the center of diopside/augite, which is confirmed to be the spinel phase ($(Mg,Fe,Mn)(Al,Cr,Fe)_2O_4$). This phenomenon proves that the crystallization of diopside/augite is induced by spinel. The Ca-rich regions observed along the grain boundaries of diopside/augite can be confirmed as the anorthite phase, which is related to the high calcium content of BFS. During the nucleation and crystallization of glass-ceramics, the remaining glassy matrix contains a certain amount of Ca^{2+} ions which possess limited mobility due to the larger radius, Si^{4+} and Al^{3+} ions combine with Ca^{2+} ions to precipitate anorthite.

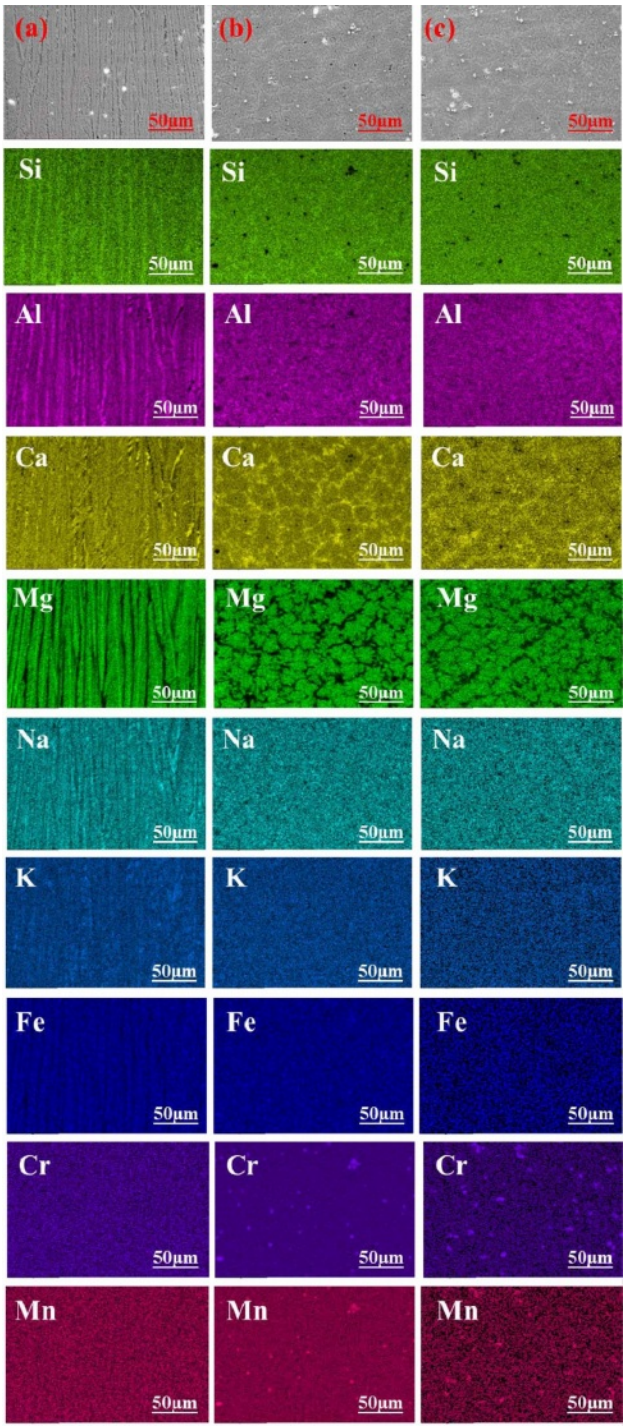

Fig. 4. SEM images: (a) FC1; (b) FC3; (c) FC5 and the element-distribution mapping.

Raman spectroscopy

It can be seen that the presence of nucleating agents Fe_2O_3 and Cr_2O_3 has a large effect on the nucleation and crystallization of glass-ceramics based on the analysis herein. A study of the effects of Fe_2O_3/Cr_2O_3 ratios on the glass network structure is helpful to deepen the understanding of the crystallization characteristics of glass-ceramics. In this study, the influence of different Fe_2O_3/Cr_2O_3 ratios on silicate network depolymerization was investigated using Raman spectroscopy and Fig. 5 shows the Raman spectra of quenched glasses. A strong and broad Raman band of 800-1200 cm^{-1} corresponds to the antisymmetric stretching of the nonbridging oxygen (NBO; $Si–O^-$) and bridging oxygen (BO; $Si–O^0$), which is formed by different structural units of Q^n in a silicate network [22-24]. Q^n describes the average number of BO atoms per silica tetrahedron and the number of BO indicated the connectivity of the silicate network [25-27]. For example, Q^0, Q^1, Q^2, and Q^3 represent $[SiO_4]^{4-}$ (4 NBO atoms, monomer), $[Si_2O_7]^{6-}$ (3 NBO atoms, dimer), $[SiO_3]^{4-}$ (2 NBO atoms, chain), and $[Si_2O_5]^{2-}$ (1 NBO atom, sheet), respectively [13, 28, 29]. In this study, based on a Gaussian function, the Raman spectra from 800 to 1200 cm^{-1} in Fig. 5 were

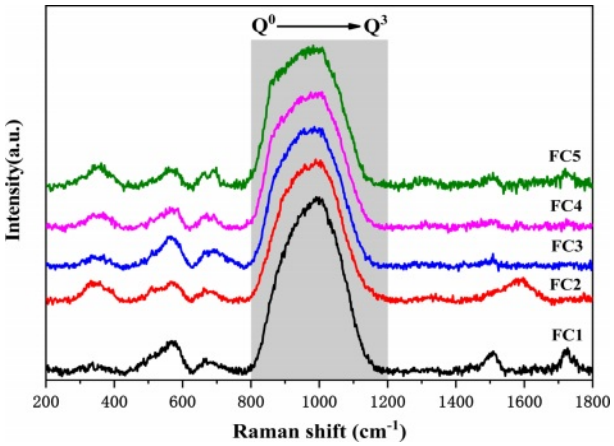

Fig. 5. Raman spectra of quenched glass samples with different Fe_2O_3/Cr_2O_3 ratios.

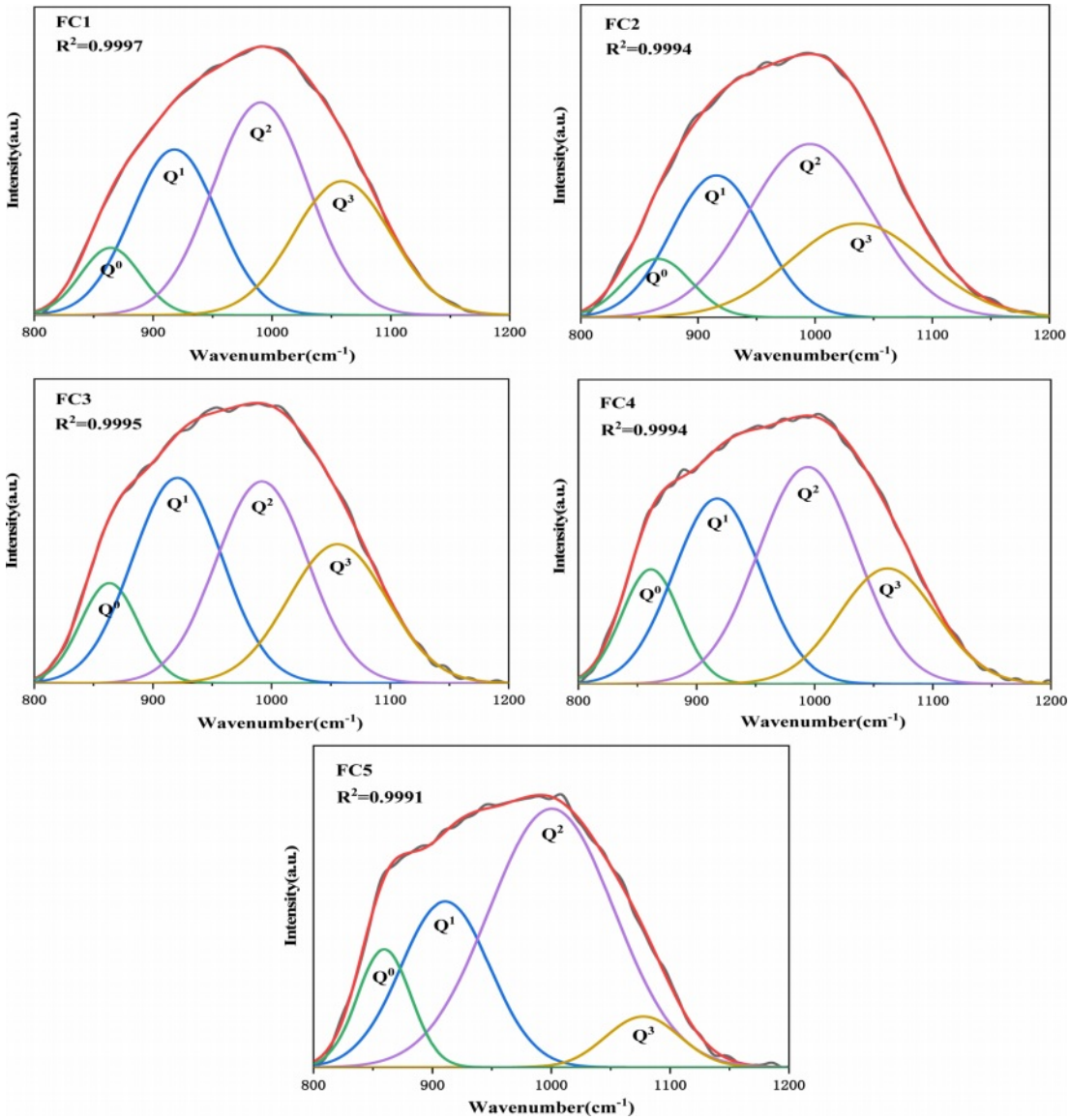

Fig. 6. Typical deconvolution of the Raman spectra of the quenched glass samples.

deconvoluted using the PeakFit software. The results are represented in Fig. 6 and the peaks at 864, 918, 990, and 1059 cm^{-1} correspond to structural units Q^0, Q^1, Q^2, and Q^3, respectively. Accordingly, Fig. 7 shows the quantitative data for the fraction of each Q^n in a silicate network with different Fe_2O_3/Cr_2O_3 ratios. It can be seen that the relative content of Q^0 shows an upward trend and the relative content of Q^3 shows a relatively sharp downward trend, while the relative content of Q^1 remains almost unchanged. The results indicate that the polymerization degree of the silicate network shows a decreased tendency with the decrease of Fe_2O_3/Cr_2O_3 ratios. Moreover, the relative content of Q^2 shows a trend of first decreasing and then increasing, and this further confirms that sample FC3 has the lowest degree of polymerization of the silicate network, which is consistent with the highest degree of crystallization of the sample FC3.

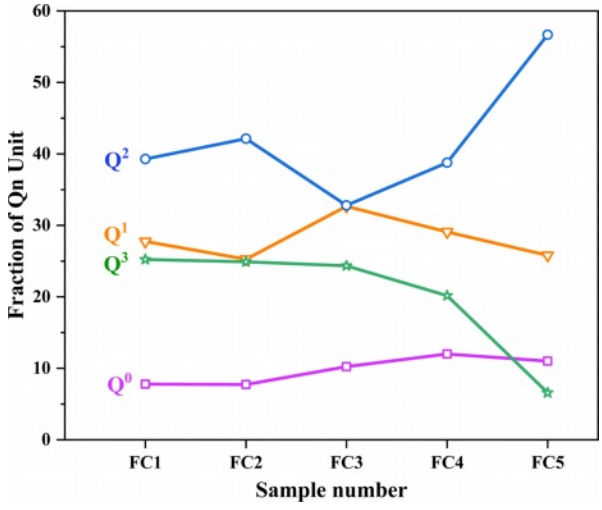

Fig. 7. Percentage of the Q^n (n=0, 1, 2, 3) structural units with different Fe_2O_3/Cr_2O_3 ratios.

Crack propagation and fracture behavior

The study of indentation-induced radial crack propagation was carried out on a Victorinox indentation instrument under a load of 4.9 N and the results are shown in Fig. 8. In samples FC1 and FC2, cracks are produced not only along the diagonal direction of the diamond-shaped indentation, but propagated along the boundary of the crystals. Thus, the main propagation way of cracks includes both transgranular and intergranular propagations, whereas intergranular crack propagation in samples FC1 and FC2 may even result in cracking and peeling on the surface [30-32], possibly because the grain boundary atomic bond-breaking behavior occurs more easily than that of grain. As a result, crack propagation along the grain boundary has a negative effect on the properties of the material in this experiment. By contrast, compared with the interconnected grain boundary in samples FC1 and FC2, the grain boundary character distribution of samples FC3, FC4, and FC5 can be found in the distribution of isolated islands which comes from the fact that the grains with different directions occlude each other in these samples. Consequently, the main mode of crack propagation in samples FC3, FC4, and FC5 is transgranular propagation and therefore the average crack length is shortened. It is noteworthy that the average crack length of sample FC5 is larger than that in samples FC3 and FC4, which may be due to the decrease of crystalline degree of diopside with excessive addition of Cr_2O_3.

To study the fracture characteristics of glass-ceramics further, SEM images of fractured surfaces of the glass-ceramics after measuring the bending strength are shown in Fig. 9. Generally speaking, the fracture mode and fracture behavior have been found to depend on both the grain boundary character distribution and crystalline degree in glass-ceramics. It can be seen that intergranular fracture is the main fracture mode in samples FC1 and FC2 because the interface between the residual glass and the residual grains is not damaged. Meanwhile, large cracks along grain boundaries are observed, revealing intergranular fracture occurrence. With the decrease of Fe_2O_3/Cr_2O_3 ratios, the interconnected grain boundary in glass-ceramic is restricted because the dendrite structure of diopside/augite crystals becomes more interlocked. Meanwhile, the fracture modes are

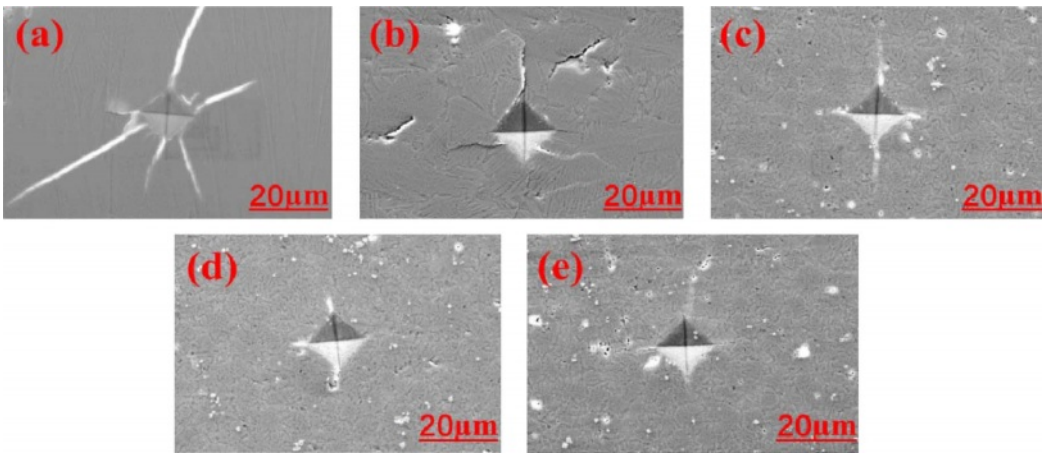

Fig. 8. Vickers impression morphology of glass-ceramics with different Fe_2O_3/Cr_2O_3 addition: (a) FC1; (b) FC2; (c) FC3; (d) FC4; (e) FC5.

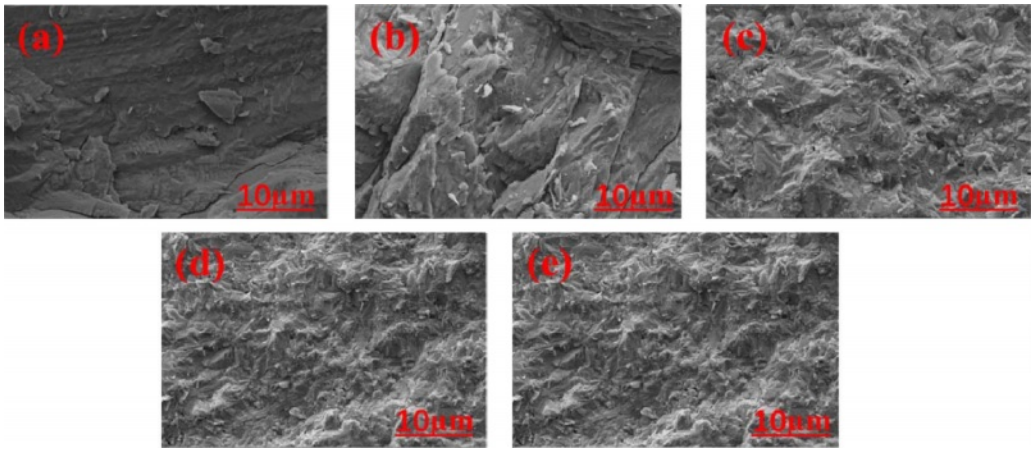

Fig. 9. SEM micrographs of the fractured surfaces with different Fe_2O_3/Cr_2O_3 addition: (a) FC1; (b) FC2; (c) FC3; (d) FC4; (e) FC5.

changed, namely, from intercrystalline to mixed transcrystalline/intercrystalline in samples FC3, FC4, and FC5. As a result, the crack growth is restrained and the fracture strength of glass-ceramics can be improved.

Corrosion resistance

Fig. 10 presents the BSE elemental mapping images of samples FC1, FC3, and FC5 in sulfuric acid solution after 5 days. In general, the corrosion resistance of the glass-ceramic is mainly determined by ion exchange between metal ions in glass-ceramic and H^+ in acid solution. Because the effect of the solidification and stabilization of metal ions by the glass phase is much less than that of the crystalline phase, the glass phase is easily corroded by acid solutions. However, diopside/augite and spinel crystals remain almost unchangeable in the process of corrosion because metal ions can stably exist in the crystalline phase by forming strong chemical bonds. The results show that there was a good effect of spinel on the immobilization of Cr and Mn, which can prevent heavy metals from polluting the environment. However, the Ca-rich regions, corresponding to anorthite, have no obvious characteristic of enrichment of Ca after corrosion which indicates that anorthite is easily corroded by sulfuric acid [33]. The results show that the corrosion resistance of diopside/augite and spinel are superior to that of anorthite. Note also that corrosion cracks at the grain boundaries can be observed compared with the results of samples without acid corrosion in Fig. 4. Usually, due to the thermal expansion mismatch between the crystal phase and the glass phase, microcracks can be observed at the grain boundaries and corrosion along microcracks occurs easily, which promotes the propagation of microcracks and the generation of new corrosion cracks [34-36]. It can be seen that the dendrites are arranged regularly in the direction of the main axis in sample FC1, and thus the grain boundaries appear as interconnected straight lines, which make the grain boundaries more susceptible to corrosion. In contrast, the diopside/augite crystals in FC3 and FC5 show an interlocking characteristic, which is beneficial to improving the grain boundary corrosion resistance and crack resistance of glass-ceramic.

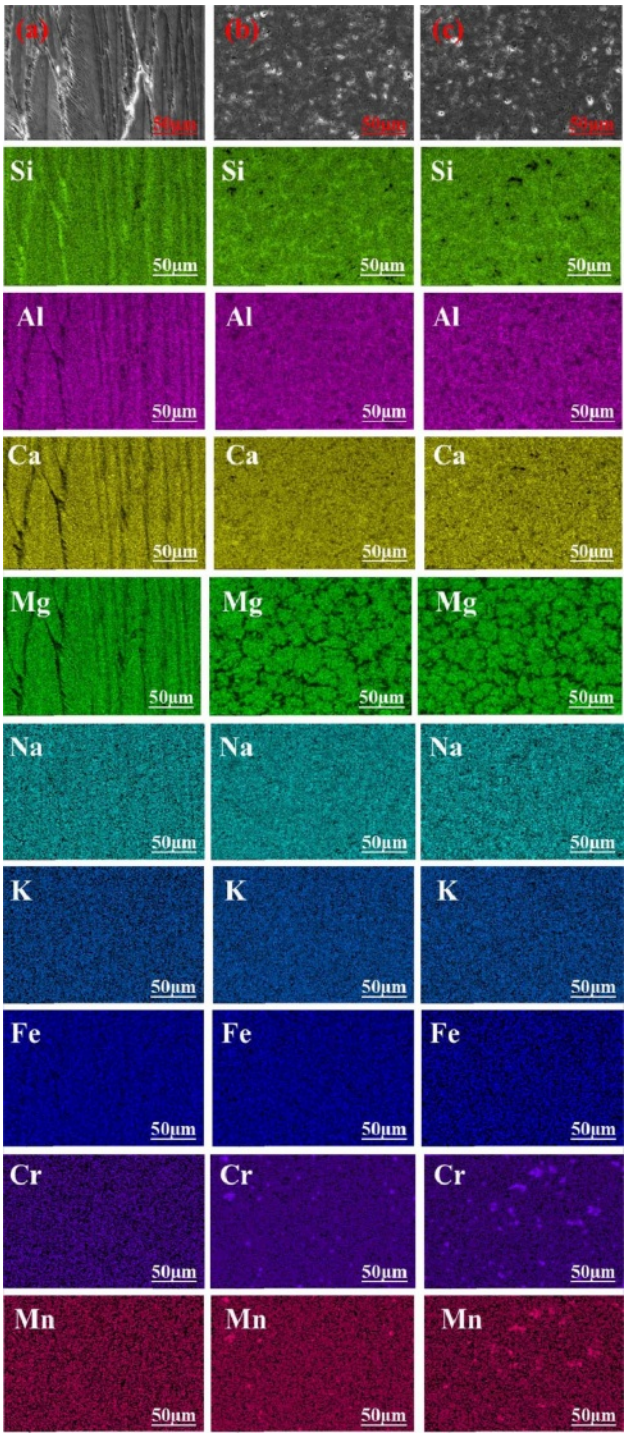

Fig. 10. BSE images and element-distribution mapping in 20 wt.% sulfuric acid solution for 5 days: (a) FC1; (b) FC3; (c) FC5.

Physical, mechanical and chemical characteristics of glass-ceramic

Table 3 shows the physicochemical properties of glass-ceramics with different Fe_2O_3/Cr_2O_3 ratios. It can be seen that the Vickers hardness, acid resistance, and bending strength of glass-ceramics tend to first increase and then decrease. Generally speaking, crystallization degree, crystalline types, and crystal morphology will affect the Vickers hardness, acid corrosion resistance, and bending strength of glass-ceramics [37-38]. With the decrease of Fe_2O_3/Cr_2O_3 ratios, the crystallization mode of glass-ceramics changes from surface crystallization to bulk crystallization, and the crystallization degree of the main crystalline phases tends to first increase and then decrease. Meanwhile, the crystal morphology is gradually converted from developed dendrite with high aspect ratios into the leaf-like morphology and then into a short rod-like shape. Note also that the main crystalline phase of glass-ceramics changes gradually from augite to diopside with the decrease of Fe_2O_3/Cr_2O_3 ratios. In another study, Li et

Table 3. Properties of glass-ceramic with different Fe_2O_3/Cr_2O_3 ratios

	FC1	FC2	FC3	FC4	FC5
Density (g/cm^3)	3.11	3.04	3.08	3.04	2.99
Hardness (GPa)	5.32	6.32	7.51	7.29	6.45
Acid-resistance (%)	95.34	94.75	97.75	95.63	94.88
Bending strength (MPa)	11.12±1.28	51.44±4.73	138.93±15.2	135.00±43.71	134.13±53.77

al. [39] reported that iron ions in ceramics could dissolve into pyroxene, resulting in the transformation of diopside to augite. Salama et al. [40] observed augite demonstrated better properties than diopside. These finding agree with the observation of our present work. The above results show the combined effects of Fe_2O_3 and Cr_2O_3 on the structure and properties of glass-ceramics. That is, the proper amount of Cr_2O_3 can strongly promote the bulk crystallization of glass-ceramics with an integrated interlocking crystal structure. Meanwhile, the addition of Fe_2O_3 contributes to the formation of augite. Above all, sample FC3 with integrated interlocking crystal structure possesses the most optimal combination of properties.

Conclusion

Glass-ceramics were successfully prepared from Baotou steel blast furnace slag and the combined effect of Fe_2O_3 and Cr_2O_3 on the structure and properties of the glass-ceramics were investigated. The following conclusions were obtained:

1. With the decrease of Fe_2O_3/Cr_2O_3 ratios, the degree of crystallization of glass-ceramics showed a trend of decreasing first and then increasing and the crystallization mode of glass-ceramics changed from surface crystallization to bulk crystallization. Accordingly, the microstructure was refined from slender dendrite to interlocking rod-shaped crystal.

2. The crystalline phases of glass-ceramics were mainly composed of diopside/augite, spinel and anorthite. The increase in Fe_2O_3/Cr_2O_3 ratios was helpful to the precipitation of augite with excellent mechanical properties. The combined effect of Fe_2O_3 and Cr_2O_3 can effectively induce the formation of augite with integrated interlocking crystal structure and the glass-ceramic showed excellent physicochemical properties with Fe_2O_3/Cr_2O_3 ratio of 1.

3. The spinel phase containing heavy metals of Cr and Mn had strong corrosion resistance in sulfuric acid, which can effectively avoid the pollution of heavy metals to the environment.

Acknowledgements

This work was supported by National Natural Science Foundation of China (grant number 52060021), Natural Science Foundation of Inner Mongolia Autonomous Region (grant number 2018MS05033) and Inner Mongolia Major Basic Research Open Project (grant number 0406091701).

References

1. T.Y. Liu, C.W. Lin, J.L. Liu, L. Han, C. Li, X. Zhou, H. Tang, Q.F. Yang, and A.X. Lu, Ceram. Int. 44[12] (2018) 14393-14400.
2. L.B. Deng, X.F. Zhang, M.X. Zhang, X.L. Jia, Z. Zhang, and B.W. Li, J. Alloys Compd. 785 (2019) 932-943.
3. C.P. Xi, J.M. Zhou, F. Zheng, J.M. Gao, P.F. Hu, Y. Li, Q. Zhen, S. Bashir, and J.L. Liu, J. Environ. Manage. 261 (2020) 110197.
4. W.Z. Liu, S. Yin, D.M. Luo, G.Q. Zhang, H.R. Yue, B. Liang, L.M. Wang, and C. Li, J. Alloys Compd. 774 (2019) 1151-1159.
5. Y. Zhao, D.F. Chen, Y.Y. Bi, and M.J. Long, Ceram. Int. 38[3] (2012) 2495-2500.
6. L.B. Deng, X.F. Zhang, M.X. Zhang, X.L. Jia, Z. Zhang, and B.W. Li, J. Alloys Compd. 785 (2019) 932-943.
7. G.A. Khater, Ceram. Int. 37[7] (2011) 2193-2199.
8. M. Rezvani, B. Eftekhari-Yekta, M. Solati-Hashjin, and V.K. Marghussian, Ceram. Int. 31[1] (2005) 75-80.
9. Y. Shi, B.W. Li, M. Zhao, and M.X. Zhang, J. Am. Ceram. Soc. 101[9] (2018) 3968-3978.
10. E. Mohaghegh, A. Nemati, B.E. Yekta, S. Banijamali, and F. Rezaei, J. Non Cryst. Solids. 408 (2015) 130-136.
11. X. He, C. Li, J.L. Liu, Q.X. Huang, X.F. Shen, T.Y. Liu, and A.X. Lu, J. Non-Cryst. Solids. 529 (2020) 119779.
12. V.K. Marghussian, O.U. Balazadegan, and B. Eftekhari-Yekta, J. Alloys Compd. 484[1-2] (2009) 902-906.
13. L.B. Deng, X.F. Zhang, M.X. Zhang, and X.L. Jia, J. Non-Cryst. Solids. 500 (2018) 310-316.
14. Y. He, X.F. Shen, Y. Jiang, and A.X. Lu, Mater. Chem. Phys. 258 (2021) 123865.
15. F.J. Pei, G.H. Zhu, P. Li, H.W. Guo, and P.Yang, Ceram. Int. 46[11] (2020) 17825-17835.
16. X.Z. Ren, W. Zhang, Y. Zhang, P.X. Zhang, and J.H. Liu, Trans. Nonferrous Met. Soc. China. 25 (2015) 137-145.
17. M.Z. Zhao, J.W. Cao, Z. Wang, and G.H. Li, J. Non-Cryst. Solids. 513 (2019) 144-151.
18. Y.C. Wang, W.W. Yu, J.L. Zhang, G.P. Luo, and Q. Jiang, Trans. Mater. Heat Treat. 35[1] (2014) 88-93.
19. T.Y. Liu, C. Li, Q.X. Huang, C.X. Liu, C.W. Lin, Q. Zhang, Z.W. Luo, L.G. Zhu, and A.X. Lu, J. Non-Cryst. Solids. 543 (2020) 120154.
20. H.R. Li, S.Y. Liu, W.C. Xu, Y.X. Zhang, Y. Shi, J. Ma, S.L. Ouyang, and Y.S. Du, J. Eur. Ceram. Soc. 41[2] (2020) 1603-1612.
21. X.W. Miao, X.T. Huo, L. Liu, S.J. Tang, M. Guo, F.Q. Cheng, and M. Zhang, Ceram. Int. 46 (2020) 15314-15324.
22. Y. Yang, T.H. Wang, Z.Y. Zhang, Z.K. Ke, C.L. Shan, X. Cao, L.Y. Ma, and S. Peng, Chem. Eng. J. 385 (2020) 123844.
23. Y.S. Du, J. Ma, X.F. Zhang, H.X. Zhang, H. Chen, S.L.

Ouyang, and B.W. Li, J. Ceram. Process. Res. 20[4] (2019) 401-410.
24. S.L. Ouyang, Y.X. Zhang, Y.X. Chen, Z.W. Zhao, M. Wen, B.W. Li, Y. Shi, M.Z. Zhang, and S.L. Liu, Sci. Rep. 9 (2019) 1964.
25. H.X. Li, B.W. Li, L.B. Deng, P.F. Xu, Y.S. Du, S.L. Ouyang, and Z.X. Liu, J. Eur. Ceram. Soc. 39[4] (2019) 1389-1396.
26. H.X. Li, B.W. Li, L.B. Deng, P.F. Xu, Y.S. Du, and S.L. Ouyang, J. Eur. Ceram. Soc. 38[6] (2018) 2632-2638.
27. M. Liu, L.J. Zhao, Y. Liu, Z.J. Lan, L.F. Chang, Y.M. Li, and H.Yu, J. Mater. Sci. Technol. 30[12] (2014) 1213-1216.
28. M.T. Wang, J.S. Cheng, B. Li, and F. He, Physica B. 406 [20] (2011) 3865-3869.
29. R.D Jia, L.B. Deng, F. Yun, H. Li, X.F. Zhang, and X.L. Jia, Mater. Chem. Phys. 233 (2019) 155-162.
30. T.E. Karakasidis and M. Meyer, Phys. Rev. B. 55 (1997) 13853-13864.
31. P. Kavouras, C. Charitidis, and T. Karakostas, J. Non-Cryst. Solids. 352[52-54] (2006) 5515-5521.
32. C.A. Charitidis, T.E. Karakasidis, P. Kavouras, and T. Karakostas, J. Phys. Condens. Matter. 19[26] (2007) 266209.
33. T.T. Wu, G.J. Liu, Y.F. Li, Y.Q. Zhang, M.M. Zhang, and B.L. Wu, J. Mater. Res. Technol. 9[3] (2020) 6287-6296.
34. Y.S. Du, J. Ma, Y. Shi, X.F Zhang, H.X. Zhang, H. Chen, S.L. Ouyang, and B.W. Li, J. Non-Cryst. Solids. 532 (2020) 119880.
35. Y. Iqbal and W.E. Lee, J. Am. Ceram. Soc. 83[12] (2000) 3121-3127.
36. X.Z. Ren, W. Zhang, Y. Zhang, P.X. Zhang, and J.H. Liu, Trans. Nonferrous Met. Soc. China. 25[1] (2015) 137-145.
37. P Ván, C Papenfuss, and W Muschik, J Phys A. 37[20] (2004) 5315-5328.
38. H. Chen, B. W. Bao, M. Zhao, X.F. Zhang, and Y.S. Du, J. Chin. Ceram. Soc. 43[9] (2015) 1240-1246.
39. Y. Li, L.H. Zhao, Y.K. Wang, and D.Q. Cang, Int. J. Miner. Metall. Mater. 25[4] (2018) 413-419.
40. S.N. Salama, H. Darwish, and H.A. Abo-Mosallam, J. Eur. Ceram. Soc. 25[7] (2005) 1133-1142.